Cone-beam Reconstruction on a Circular Short-Scan using the Factorization Approach

Frank Dennerlein, Frédéric Noo, Harald Schöndube, Joachim Hornegger, and Günter Lauritsch

***Abstract*— In this article, we present a novel, truncation-flexible cone-beam (CB) reconstruction algorithm for the short-scan circular trajectory, which is based on the theoretically-exact factorization theory previously derived by our group. The factorization theory demonstrates how to decompose the 3D CB reconstruction problem into a family of independent 2D inversion problems. Here, we use a numerical approach based on a constrained conjugate gradient least-squares iteration scheme to find solutions to the 2D problems. We present reconstructions from computer-simulated CB data and evaluate the reconstruction behavior in terms of CB artifacts. Image results are compared to reconstructions using the short-scan Feldkamp algorithm.**

I. Introduction

Circular cone-beam (CB) computed tomography (CT) has become a powerful tool in the clinical arena. 3D image reconstruction on state-of-the-art scanning systems is typically based on an algorithm that has been heuristically derived by Feldkamp *et al.* [1]. For data collected along a 360-degrees scan (full scan), the Feldkamp reconstruction method (FDK) can be set into a firm theoretical context and yields often acceptable image quality. The mechanical design of established medical C-arm devices, however, does not usually allow a full scan. To apply FDK with data acquired along less than 360-degrees (short-scan), the issue of data redundancy is handled using Parker-like weighting methods [2]. In general, however, these weighting schemes are a significant approximation, since they neglect the cone-angle and therefore treat distinct data as redundant. This approximation often results in a high level of CB artifacts in the reconstructed images for regions outside the plane of the circle scan (abbreviated as PCS in the following).

Recently, we introduced a novel CB inversion theory for the circular short-scan trajectory [3]. It is based on the factorization of the 3D reconstruction problem into a set of independent 2D inversion problems and lies on an exact theoretical background. In this article, we develop a CB reconstruction algorithm using the theory from [3] while applying an iterative approach to invert the 2D problems. Whereas in [3], no direct reconstruction from CB data was shown, we now present reconstructions from computer simulated CB data and compare the performance of the algorithm to that of the short-scan FDK method.

F. Dennerlein, F. Noo and H. Schöndube are with the Department of Radiology, University of Utah, Salt Lake City, Utah, USA

E-mail: fdenner@ucair.med.utah.edu

J. Hornegger is with the Institute of Pattern Recognition, University of Erlangen-Nuremberg, Erlangen, Germany

G. Lauritsch is with Siemens AG, Medical Solutions, Forchheim, Germany.

This work was partially supported by a grant of Siemens AG, Medical Solutions and by the U.S. National Institutes of Health (NIH) under grant R01 EB000627.

II. Acquisition Geometry and Notation

We use the notation $\underline{a}(\lambda) = (R\cos\lambda, R\sin\lambda, 0)^T$ to describe the circular trajectory of radius R followed by the focal spot of the X-ray source during data acquisition. The curve parameter λ is bounded in $[0, \lambda_{max}]$ and since our studies are restricted to short-scans, we require $\lambda_{max} < 2\pi$. The spatial distribution of the linear X-ray attenuation coefficient of the interrogated object is represented using the function $f(\underline{x})$ with $\underline{x} \in I\!R^3$. We assume that f is compactly supported in a cylinder with axis $(0,0,1)^T$ and circular base of radius R_{obj}, where $R_{obj} < R$. CB projection data of the object are acquired using an X-ray sensitive 2D detector. During the scan, we measure integrals of f along rays, with each ray connecting the X-ray source for a given λ with an arbitrary point on the detector. Hence, we obtain samples of the data function

$$g(\lambda, \underline{\alpha}) = \int_0^\infty f(\underline{a}(\lambda) + t\underline{\alpha})\, dt, \tag{1}$$

with the vector $\underline{\alpha}$ describing ray directions. Analog to [3], the

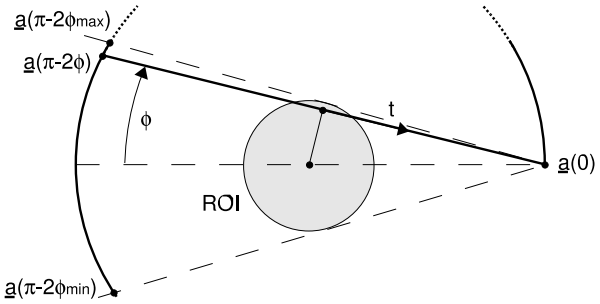

Fig. 1. Illustration of the Φ-plane family (orthogonal projection onto the PCS).

image volume is represented with a non-Cartesian coordinate system, which is based on the one-parametric family of Φ-planes: Each Φ-plane is orthogonal to the PCS and contains the source position $\underline{a}(0)$, at the beginning of the short-scan. The parameter Φ describes the angle between the Φ-plane and the line connecting the origin $(0,0,0)^T$ with $\underline{a}(0)$. The angle Φ increases in clockwise direction, is bounded in $[\Phi_{min}, \Phi_{max}]$ and becomes $\Phi = 0$ for the Φ-plane that contains the rotation axis. The interval for Φ is selected such that the set of Φ-planes covers the complete region of interest (ROI). Assuming a circular scan of adequate length ($\lambda_{max} \geq \pi - 2\Phi_{min}$), each Φ-plane intersects the source trajectory twice: at $\underline{a}(0)$ and at curve parameter $\lambda_o(\Phi) = \pi - 2\Phi$. A Cartesian (t, z)-coordinate system is introduced on each Φ-plane, with t orthogonal to $(0,0,1)^T$ and z parallel to the axis of rotation. The coordinate t becomes 0 at the orthogonal projection of

$(0,0,0)^T$ onto the Φ-plane and increases when approaching $\underline{a}(0)$ (see Fig. 1). An arbitrary point in the ROI can be parametrized with coordinates (Φ, t, z) with a change of variable to Cartesian coordinates provided by the function

$$\underline{x}_\Phi(t,z) = \begin{pmatrix} R\sin^2\Phi + t\cos\Phi \\ R\sin\Phi\cos\Phi - t\sin\Phi \\ z \end{pmatrix}. \tag{2}$$

III. Reconstruction Theory

The factorization method is based on the theoretically-exact decomposition of the 3D CB reconstruction problem into a family of independent 2D inversion problems [3]. The decomposition applies to a full-scan as well as to a short-scan trajectory and significantly reduces the total complexity of the reconstruction task. Each of the 2D problems corresponds to finding the object density on a given Φ-plane, i.e. the function

$$f_\Phi(t,z) = f\left(\underline{x}_\Phi(t,z)\right). \tag{3}$$

A single 2D inversion problem is established as shown in [3]: By backprojecting the locally filtered CB data $\frac{\partial}{\partial\lambda} g(\lambda, \underline{\alpha})$ onto a fixed Φ-plane using only the scan segment $\lambda \in [0, \lambda_o(\phi)]$, an intermediate function $b_\Phi(t,z)$ is obtained. The equation

$$\frac{1}{\pi} b_\Phi(t,z) = \int_{-\infty}^{+\infty} dt' h_H(t-t') \times \\ \times \left(f_\Phi\left(t', z_1(t')\right) + f_\Phi\left(t', z_2(t')\right)\right) \tag{4}$$

then relates $b_\Phi(\cdot,\cdot)$ to the sought object function $f_\Phi(\cdot,\cdot)$ [4]. In (4), $h_H(\cdot)$ denotes the Hilbert filter kernel in spatial domain. Also, $z_1(\cdot)$ and $z_2(\cdot)$ define filter directions in the Φ-plane that truly also depend on Φ, t and z. More specifically, the points $\underline{x}_\Phi\left(t', z_1(t')\right)$ are located on the line connecting $\underline{a}(0)$ with $\underline{x}_\Phi(t,z)$ and correspondingly, the points $\underline{x}_\Phi\left(t', z_2(t')\right)$ are located on the line connecting $\underline{a}(\lambda_o(\Phi))$ with $\underline{x}_\Phi(t,z)$. Reconstruction of object density on the Φ-plane corresponds to solving (4) for $f_\Phi(\cdot,\cdot)$. The complete ROI is reconstructed by varying Φ and repeating the steps explained earlier in this paragraph.

It is known, however, that data along a planar trajectory is in general not sufficient for theoretically-exact and stable 3D CB reconstruction outside the PCS, (see [5] and others). Hence, reconstruction of $f_\Phi(t,z)$ for $z \neq 0$ suffers from missing data, so that edges in z direction cannot be resolved accurately. Let us now consider the special case that $f_\Phi(t,z)$ is independent of z. Then, for each point (t,z) we have $f_\Phi\left(t', z_1(t')\right) = f_\Phi\left(t', z_2(t')\right) = f_\Phi\left(t', 0\right)$. Therefore, the right hand side (RHS) of (4) can be reduced to the 1D convolution $2\int_{-\infty}^{+\infty} dt' h_H(t-t') f_\Phi\left(t', 0\right)$. Reconstruction of $f_\Phi(t,z)$ then becomes equivalent to the problem of reconstructing $f_\Phi(t,0)$, for which a theoretically-exact and stable solution can be found. In conclusion, the object density at a point $\underline{x}$ that is not located on the PCS can be recovered accurately, if $\underline{x}$ belongs to a Φ-plane on which the object density is independent of z (see Fig. 2). In general, however, solving (4) for $f_\Phi(\cdot,\cdot)$ constitutes an ill-posed problem. We try to stabilize the inversion by (i) introducing additional constraints on the solution $f_\Phi(\cdot,\cdot)$ and (ii) by using regularization techniques to reduce the ill-posedness of the 2D inversion problem. The following constraints on $f_\phi(\cdot,\cdot)$ are considered:

CRAY: Knowledge about integrals of $f_\Phi(\cdot,\cdot)$ along rays diverging from $\underline{a}(0)$ and $\underline{a}(\lambda_o(\Phi))$. These integrals are part of the acquired CB data.

CPOS: Knowledge that $f_\Phi(\cdot,\cdot)$ is a non-negative function, since it represents object density.

CADD: This constraint overcomes the problem of missing data on a substantial level by extending the source trajectory. We now introduce an additional line scan $\mathcal{L}$ that is attached at $\underline{a}(0)$ and perpendicular to the PCS (see Fig.2). However, CB data acquired along $\mathcal{L}$ is not processed using a filtering-and-backprojection scheme as in [4]. It is rather used in a similar fashion as in CRAY to put additional constraints on $f_\Phi(\cdot,\cdot)$. This allows a very coarse sampling of $\mathcal{L}$ with as few as only one additional CB projection, if desired.

IV. 2D Inversion Approach

Reconstruction of $f_\Phi(\cdot,\cdot)$ is achieved by discretizing (4) and applying a numerical inversion method. Following the strategy of [3], we introduce the vectors $\underline{f}$ and $\underline{b}$ that denote samples of the functions $f_\Phi(\cdot,\cdot)$ and $b_\Phi(\cdot,\cdot)$ and compose a linear system of equations $M\underline{f} = \underline{b}$ that represents (4). To satisfy Shannon's sampling theory, a band-limited version of the Hilbert filter kernel in (4) is applied using a rectangular apodization window and cut-off frequency $b = 1/(2\Delta t)$. In spatial domain, the band-limited filter is given as

$$h_H^b(t) = \frac{1}{\pi t}\left(1 - \cos\frac{\pi t}{\Delta t}\right) \tag{5}$$

and a sampling at the required parameters $k\Delta t$ with $k \in Z$ yields

$$h_H^b(k\Delta t) = \begin{cases} \frac{2}{\pi k \Delta t} & \text{if } k \text{ is even,} \\ 0 & \text{if } k \text{ is odd or } k = 0. \end{cases}$$

Since every other sample of $h_H^b(\cdot)$ becomes 0, a straightforward application of the discrete convolution implies a suboptimal use of data and a loss in resolution. To overcome

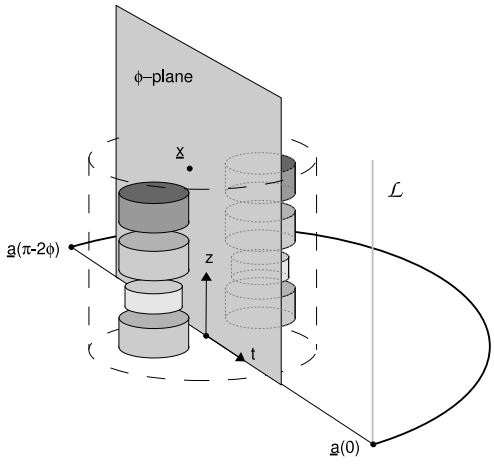

Fig. 2. On the illustrated Φ-plane, the object density is independent of z. Therefore, reconstruction of the corresponding function $f_\Phi(\cdot,\cdot)$ constitutes a well-posed problem. In the general case, we optionally consider CB data for an additional line scan $\mathcal{L}$ to stabilize the 2D inversion problem.

this problem, we oversample in t by a factor of 2 on every Φ-plane, by duplicating each sample of b_Φ prior to inversion. The oversampling is compensated by a corresponding averaging operation in the resulting $\underline{f}$. Reconstructed images with and without the oversampling strategy are presented in Section V.

The discrete modeling allows a straight-forward handling of the constraints CRAY and CADD. We extend the linear system by adding equations that represent the knowledge about additional ray integrals of $f_\Phi(\cdot,\cdot)$ to obtain

$$A\underline{f} := \begin{bmatrix} M \\ \beta_1 C_1 \\ \beta_2 C_2 \end{bmatrix} \underline{f} = \begin{bmatrix} \underline{b} \\ \beta_1 \underline{c}_1 \\ \beta_2 \underline{c}_2 \end{bmatrix} := \underline{d}. \tag{6}$$

In (6), the submatrix C_1 corresponds to equations for CRAY, C_2 corresponds to equations for CADD and $\underline{c}_1$ and $\underline{c}_2$ denote samples of the corresponding ray integrals. The coefficients β_1 and β_2 allow to adjust the impact of the considered constraints.

Because the large dimension of A forbids a direct inversion, an iterative scheme is applied to find a solution to the 2D problem. In practice, the ideal data vector of the RHS of (6) is not available. Instead, we need to consider a system $A\underline{f} = \tilde{\underline{d}}$, where $\tilde{\underline{d}}$ is an approximation of the ideal $\underline{d}$ that is contaminated by discretization, quantization and noise effects. We aim at finding a non-negative, least-square (LS) estimate $\tilde{f}$ for f by applying a conjugate-gradient (CG) iteration scheme on the normal equations

$$A^T A\tilde{\underline{f}} = A^T\tilde{\underline{d}}. \tag{7}$$

CG-LS methods provide fast speed of convergence [6] and are considered to be a good choice for tomographic inversion problems because of their initial modification of the data vector with the operator A^T [7]. To account for constraint CPOS, we closely follow the projected restarted iteration scheme of [8]: a non-negative estimate $\tilde{\underline{f}}$ is determined by alternating CG-LS iterations and orthogonal projections of intermediate results onto the set of vectors with non-negative components (see Algorithm 1). The iterative inversion approach is stopped after a certain number of iterations. By that, we implicitly regularize the linear system to allow a stable and meaningful estimate $\tilde{\underline{f}}$ in the context of our ill-posed problem.

Initial estimate $\tilde{\underline{f}}^{(0)} = \underline{0}$;
for $j = 1 \dots NOUT$ **do**
  compute residual $\underline{r}^{(j)} = \tilde{\underline{d}} - A\tilde{\underline{f}}^{(j-1)}$;
  find LS estimate $\tilde{\underline{u}}^{(j)}$ for $A\underline{u}^{(j)} = \underline{r}^{(j)}$ using NIN CG-iterations ;
  update $\tilde{\underline{f}}^{(j)} = \mathcal{P}\left(\tilde{\underline{f}}^{(j-1)} + \tilde{\underline{u}}^{(j)}\right)$;

Algorithm 1: Applied iteration scheme. The operator $\mathcal{P}$ describes the projection onto vectors with non-negative components.

V. Numerical Evaluation

The suggested reconstruction algorithm is now evaluated using computer simulated CB data. We consider a typical C-arm geometry ($R = 750mm$, $\lambda \in [0, 216]$ deg., $\Delta\lambda = 0.4$ deg.) and use a virtual, planar detector that contains the rotation axis. An analytically defined disk phantom of limited vertical extent is investigated; its ground-truth is displayed in

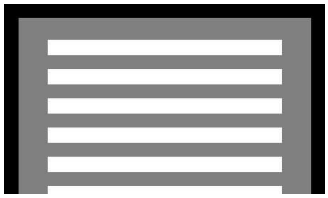

Fig. 3. True density values of the disk phantom in $[-500HU, 500HU]$.

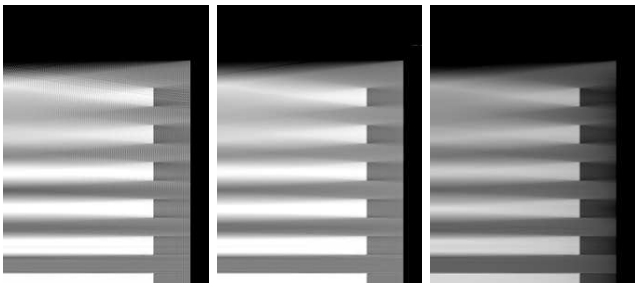

Fig. 4. The slice $\Phi = 0$ for $z \in [0, 15cm]$ through the reconstruction using parameter set 1: (left) no oversampling, but using CPOS (center) oversampling by a factor 2 in t and using CPOS, (right) oversampling, but not using CPOS. Grayscale window $[-500HU; 500HU]$

Fig. 3. Reconstructions are performed from ideal and noisy CB data and are presented next to the image results obtained with the short-scan FDK method. The investigated phantom consists of a stack of six cylindrical disks embedded in a water cylinder of radius 10 mm. Each disk has a radius of 8 cm and a thickness of 1 cm. The phantom is centered at the axis of rotation and shifted, such that the center of the lowest disk is located on the PCS. Also, it is entirely contained in the field-of-view yielding transaxially untruncated CB data.

The parameters used for reconstruction are given in set 1 in Table I. Fig. 4 illustrates the effects of the constraint CPOS and the oversampling strategy on reconstruction quality. The planes $\Phi = 0$ through reconstructions from ideal and noisy CB data are presented in Fig. 5. Results in the bottom row of Fig. 5 were obtained using the constraint CADD and four CB projections acquired along the additional line-scan $\mathcal{L}$ (see Fig. 2). The additional source positions were located at $z = \{3, 6, 9, 12\}$cm, i.e., at the gap between two disks (for $z = \{3, 9\}$cm), at the center of a disk (for $z = 6$ cm) or at the top of the phantom, respectively. Reconstructions of the slice $x = 0$ from non-noisy CB data are shown in Fig. 6. Reconstructions were obtained using parameter set 2 and bilinear rebinning of the densities from the Φ-plane coordinate system onto a Cartesian grid.

TABLE I
Evaluation Parameters

	Set 1	Set 2
detector pixel size	$0.5 \times 0.5mm^2$	$1.0 \times 1.0mm^2$
Φ-plane sampling	$0.5 \times 0.5mm^2$	$1.0 \times 1.0mm^2$
pixel columns in Φ-plane	$nt = 440$	$nt = 220$
image voxel size	$0.5 \times 0.5 \times 0.5mm^3$	$1.0 \times 1.0 \times 1.0mm^3$
constraints	$\beta_1 = 1/nt$	$\beta_1 = 1/nt$
	$\beta_2 = 10/nt$	$\beta_2 = 5/nt$
iterations $(NIN, NOUT)$	$(12, 20)$	$(12, 7)$

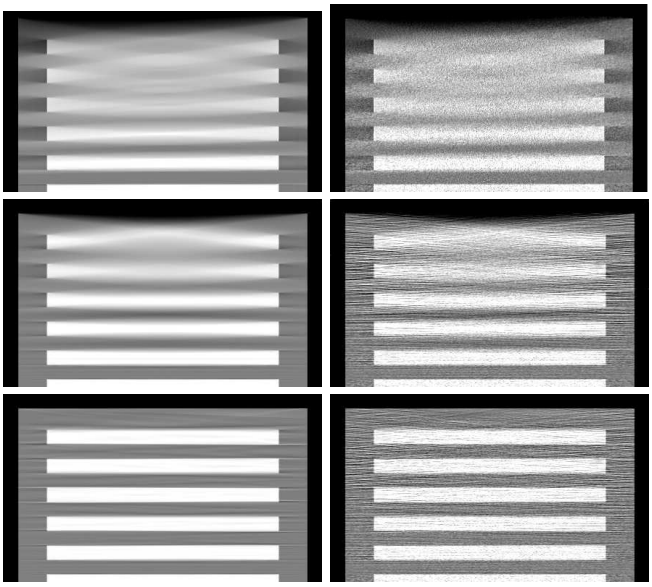

Fig. 5. Reconstruction of the slice $\Phi = 0$ with $z \in [0, 13cm]$, from (top) to (bottom): short scan FDK, factorization approach, factorization approach and 4 additional CB projections on $\mathcal{L}$. (left) using non-noisy CB data, (right) using CB data containing Poisson noise with $100,000$ photons per ray. Grayscale window $[-500HU; 500HU]$

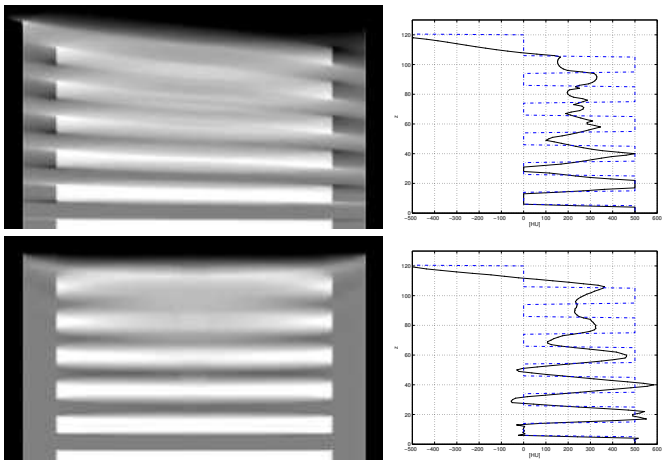

Fig. 6. Reconstruction of the slice $x = 0$ mm with $z \in [0, 13cm]$: (left) Image result in $[-500HU; 500HU]$, (right) profile along $(x, y) = (0, 0)$ compared against the true phantom values (dashed). (top) Short-scan FDK, (bottom) factorization approach.

VI. Discussion

Reconstructions of the disk phantom from a circular short-scan using the factorization approach show a remarkable reduction of CB artifacts compared to results from the short-scan FDK method: The shadow-regions enclosing each cylinder are less prominent and CB artifacts are shifted to locations more remote from the PCS. In particular, accurate reconstruction is achieved as expected for Φ-planes that do not intersect the disks (see left/right of each disk in the bottom of Fig. 6).

Fig. 4 shows that the oversampling approach adequately avoids vertical streaks in the reconstruction results (center image). Also, considering the positivity constraint CPOS contributes to more reconstruction accuracy after a constant number of iterations (compare center and right of Fig. 4).

The introduction of only four CB projections along an additional line scan improves image quality significantly and almost completely overcomes the phenomena of CB artifacts in the investigated scenario.

The right column in Fig. 5 illustrates that the factorization method is robust with respect to noise in the CB data. Its noise propagation, however, is visually of different nature compared to that of the short-scan FDK approach.

Since the factorization method requires only local filtering of CB data prior to backprojection, reconstruction from partially transaxially-truncated projections becomes feasible in practically-relevant scenarios (see also [9]). Investigations on the reconstruction behavior in presence of transaxial truncation involving the FORBILD head phantom are planned in the near future.

VII. Conclusions

We suggested a novel, flexible 3D CB reconstruction approach which is based on the theoretically-exact factorization theory from [3] and allows reconstruction from less than a short scan. The algorithm decomposes 3D CB reconstruction into a set of independent 2D inversion problems, each of which is solved numerically using a constrained conjugate gradient least-squares iteration scheme. This reduction in complexity allows an efficient, parallel implementation of the algorithm. Since a global filter operation in the projection domain is avoided, reconstruction in presence of transaxial data truncation becomes feasible in practically-relevant scenarios.

In contrast to [3], where no direct reconstruction from CB data was shown, we here presented a numerical evaluation of the suggested algorithm from computer-simulated CB data. The reconstruction results show a noticeable improvement in image quality in terms of CB artifacts compared to the short-scan FDK approach. Utilizing the flexibility of the factorization approach by considering four more CB projections acquired along an additional line scan helps to overcome the phenomena of CB artifacts almost completely in the studied scenario.

References

[1] L. A. Feldkamp, L. C. Davis, and J. W. Kress, "Practical cone beam algorithm," *Optical Society of America*, vol. 1, pp. 612–619, 1984.

[2] D. L. Parker, "Optimal short scan convolution reconstruction for fanbeam CT," *MP*, vol. 9(2), pp. 254–257, 1982.

[3] F. Dennerlein, F. Noo, J. Hornegger, and G. Lauritsch, "Factorization of the reconstruction problem in circular cone-beam tomography and its use for stability analysis," *Proceedings IEEE MIC, 2006*, vol. 4, pp. 2908–2912.

[4] J. D. Pack, F. Noo, and R. Clackdoyle, "Cone-beam reconstruction using the backprojection of locally filtered projections," in *IEEE Trans. Med. Imag. 24(1)*, 2005, pp. 70–85.

[5] H. K. Tuy, "An inversion formula for cone beam reconstruction," *SIAM J. Appl. Math.*, vol. 43(3), pp. 546–552, 1983.

[6] Y. Saad, *Iterative methods for sparse linear systems*. SIAM, 2003.

[7] D. Calvetti and E. Somersalo, "Priorconditioners for linear systems," *Inverse Problems*, vol. 21, pp. 1397–1418, 2005.

[8] D. Calvetti, G. Landi, L. Reichel, and F. Sgallari, "Non-negativity and iterative methods for ill-posed problems," *Inverse Problems*, vol. 20, pp. 1747–1758, 2004.

[9] M. Defrise, F. Noo, R. Clackdoyle, and H. Kudo, "Enlargement of the region of accurate reconstruction in computed tomography from truncated data," in *The 8th international meeting on fully three-dimensional image reconstruction in radiology and nuclear medicine*, 2005, pp. 46–49.